EXPERIMENTAL METHODS FOR STACKING FAULT OBSERVATIONS AND ENERGY MEASUREMENTS.OBSERVATION OF STACKING FAULTS BY X-RAY TOPOGRAPHY

A. Authier

OBSERVATION OF STACKING FAULTS BY X-RAY TOPOGRAPHY

A. AUTHIER

Laboratoire de Minéralogie Cristallographie (*),
Université P.-et-M.-Curie, 4, place Jussieu, 75230 Paris Cedex 05, France.

Résumé. — Après avoir brièvement rappelé les principes de la propagation des rayons X dans un cristal parfait et des techniques de topographies aux rayons X, on explique la formation de l'image d'une faute d'empilement et on montre comment ce défaut peut être complètement caractérisé. A titre d'exemple, on montre des fautes d'empilement dans un cristal de silicium contenant de l'oxygène et recuit à 1 200 °C.

Abstract. — After briefly recalling the main principles of X-ray propagation in perfect crystal and of X-ray topographic techniques, one describes the formation of stacking fault images and shows how these faults can be fully characterized. An example is shown of stacking faults in silicon crystals annealed at 1 200 °C and which contained 5×10^{17} at/cm^3 oxygen.

1. **Introduction.** — X-ray topography dates back to 1958-1959 [1, 2] (see the reviews [3] to [6]) and has proved to be a most useful tool for the characterization of localized defects in large nearly perfect crystals. In particular, a number of papers have been devoted to the observation of stacking faults in silicon [7] to [10], quartz [11] to [13], beryllium oxide [14], etc... and to the theory of their image formation [15] to [17], [13], [9].

The principles of X-ray propagation in perfect crystals and X-ray topography will be briefly recalled. It will then be showed how a stacking fault may be fully characterized on X-ray topographs.

2. **Principles of X-ray propagation in a perfect crystal.** — The principles of dynamic diffraction of waves by matter are described in the paper by R. Gevers (this volume). The particular case of X-rays is discussed at length in the book by M. von Laue [18] (see also ref. [19] and [20]).

The propagation equation of waves in matter is derived from Maxwell's equation in the case of electromagnetic waves and Schrödinger's equation in the case of electron or neutron waves. Its simplest solution when the medium is triply periodic is a Bloch wave

$$\Psi = \exp - 2\pi i \mathbf{K}_0 . \mathbf{r} \sum \Psi_h \exp 2\pi i \mathbf{h} . \mathbf{r} \qquad (1)$$

(h is a reciprocal lattice vector), which has the same periodicity as the crystal. In a perfect crystal $\mathbf{K}_0$ and Ψ_h are constant. This Bloch wave can also be written :

$$\Psi = \sum \Psi_h \exp - 2\pi i \mathbf{K}_h . \mathbf{r} \qquad (2)$$

with

$$\mathbf{K}_h = \mathbf{K}_0 - \mathbf{h} .$$

Eq. (2) shows that the solution is *a wave-field* constituted by a *sum* of waves having Ψ_h and $\mathbf{K}_h$ as amplitude and wave-vector respectively. It can be shown that the waves constituting a wave-field are strongly coupled and propagate simultaneously through the crystal, with the same path and the same absorption. This absorption is highly anomalous when the Bragg condition is satisfied.

According to the geometrical theory of diffraction, Bragg's condition is satisfied when two reciprocal lattice points at least lie on the Ewald sphere (Fig. 1). In the X-ray case, there are two points only in general. The wave-lengths $L_a O$ and $L_a H$ of the incident and reflected waves are in the geometrical theory equal to $1/\lambda$. Actually, one has to take into account the index of refraction of the medium for X-rays and the wave-vectors of waves propagating either in the incident or reflected direction are equal to n/λ far from the reflection domain : their extremity lies on spheres centered in O and H and having n/λ as radii (Fig. 2). When this point is close to the intersection of both spheres, that is when Bragg's condition is nearly satisfied, its locus is a surface asymptotic to the two sphere which is called the dispersion surface (Fig. 2). This surface plays a similar role to the surface of indices in the case of visible light. The intersection of this surface by the plane containing the two wave-vectors, $\mathbf{K}_0$ and $\mathbf{K}_h$, is a hyperbola asymptotic to the two spheres assimilated to their tangential planes on figure 3. The propagation direction of a wave-field characterized by its two waves of wave-vectors **OP** and **HP** lies along the normal to

(*) Associé au C.N.R.S.

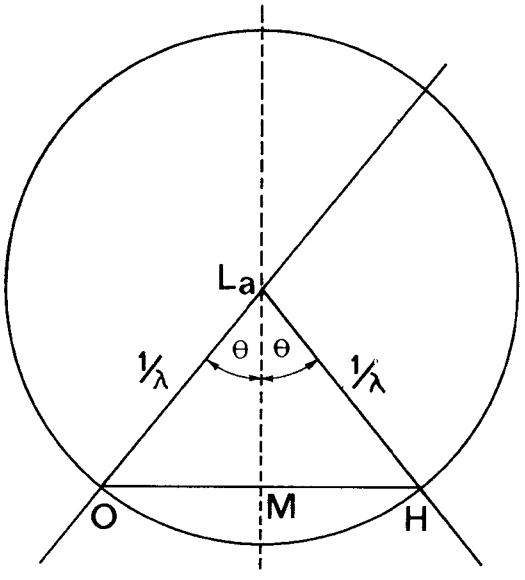

FIG. 1. — Ewald construction. LaO : incident direction ; LaH reflected direction ; **OH** reciprocal lattice vector. In triangle $La\ OM : \frac{1}{2d} = \frac{1}{\lambda} \sin\theta$.

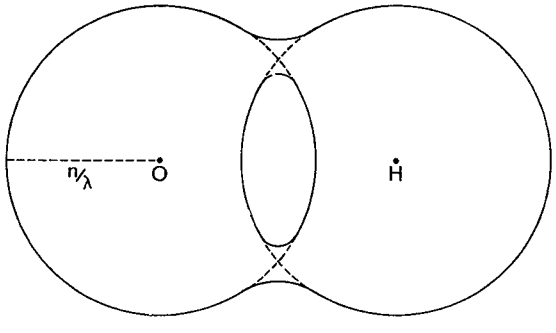

FIG. 2. — Dispersion surface.

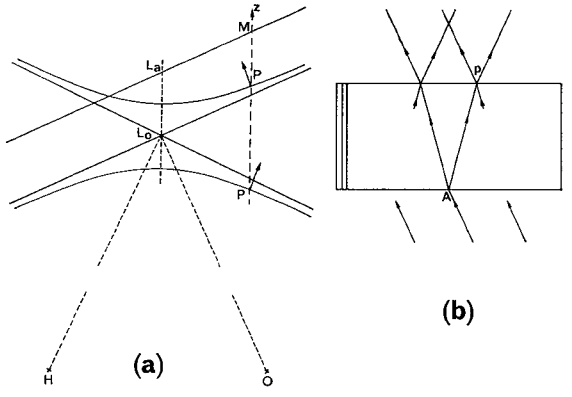

FIG. 3. — X-ray propagation in the plane wave case. *a*) Dispersion surface in the reciprocal space ; Mz : normal to the entrance surface. The arrows at P_1 and P_2 show the propagation direction of the wave-fields. *b*) Direct space.

wave generates within the crystal a whole array of wave-fields whose propagation directions inside the crystal fill out the so-called Borrmann triangle limited by the incident and reflected directions (Fig. 4). Along any

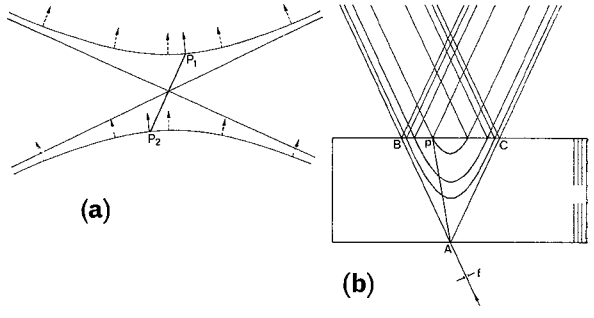

FIG. 4. — X-ray propagation in the spherical wave case. *a*) Reciprocal space. *b*) Direct space P_1 and P'_2 are the tie points of the wave-fields propagating along *Ap*.

the dispersion surface at *P*, called the tie-point. The absorption of the wave-field is smaller than the normal when *P* lies on branch 1 and higher when *P* lies on branch 2 (Borrmann effect).

Let us consider an incident plane wave with wave-vector **OM** of length $1/\lambda$. The wave-vectors of the waves it creates inside the crystal must have the same tangential component as **OM** on the crystal surface. Their extremity should therefore lie on the intersection of the normal to the crystal surface drawn from *M* with the dispersion surface. Figure 3 shows that an incident plane wave thus excites *two wave-fields* inside the crystal in the transmission case. Any point of the exit surface thus receives two wave-fields which are coherent and interfere. When each wave-field reaches the exist surface, it decouples into its two components, the refracted and the reflected waves.

In the case of X-rays however, the incident wave is always a spherical wave and all the points of the dispersion surface are simultaneously excited. The incident direction *Ap* within the triangle propagate two wave-fields characterized by points P_1 and P'_2 of the dispersion surface. These two wave-fields interfere giving rise to interference fringes in the reflected and refracted beams (the so-called *Kato* Pendellösung fringes). Since wave-fields belonging to branch 2 are more absorbed than normal, these fringes disappear when the product μt of the linear absorption coefficient μ by the crystal thickness t is larger than 4 or 5.

3. **Principles of X-ray topography.** — We shall limit ourselves here to the Lang setting (Fig. 5). The beam of X-rays emitted by a point focus ($100 \times 100\,\mu m^2$ — optical) is limited by a fine slit parallel to the reflecting planes and such that the crystal can be adjusted for Bragg reflection independently for $K\alpha_1$ and $K\alpha_2$ radiations. The direct beam has usually a divergence of 40 to 60″ which is much larger than the width of the reflection domain of the perfect crystal. After it has entered the crystal, it only contains rays which do not

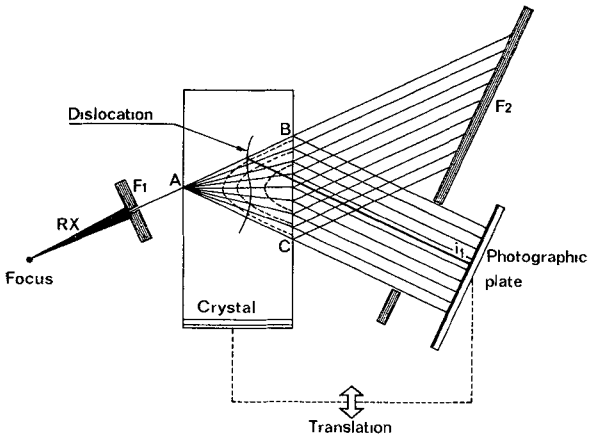

FIG. 5. — Principle of X-ray topography. F : focus ; F_1, F_2 : first and second slits ; P : photographic plate ; i_1 : direct image of the defect.

fulfill Bragg's condition for the perfect crystal. The other have given rise to the wave-fields propagating within the Borrmann triangle ABC. If the direct beam hits a defect, part of it may satisfy Bragg's condition on the distorted lattice planes around the defect and give rise to a reflected beam and an image, i_1, called the *direct* image on the photographic plate [21]. From the distance of i_1 from the edges of the trace of the reflected beam, it is easy to deduce the depth of the defect which gave rise to the images. One has thus obtained a *section* of the crystal by the incident beam of X-rays ; it is called a *section topograph*. The presence of a defect within the Borrmann triangle also perturbates the propagation of the wave-fields, giving rise to other types of images which are more complicated to explain [21] but can be simulated on a computer [22].

In order to obtain a projection of *all* the defects contained in the crystal, A. R. Lang had the idea [1, 2] to traverse simultaneously the crystal and the photographic plate ; the resulting topograph is called a *traverse*, or projection topograph. The intensity received by any point of the photographic plate is equal to the integral of the intensity distribution along the base of the Borrmann triangle, integral performed as the reflected beam goes across this point ; it is called the integrated intensity.

4. **Comparison between electron microscopy and X-ray topography.** — Although there are of course similarities of principle in the diffraction of electromagnetic waves and electrons by triply periodic matter, there are also some practical differences which it is important to point out.

The interaction of electrons which are charged with matter is much stronger than that of X-rays. This has two consequences. The first is that the index of refraction of matter for X-rays is very close to one, with the result that it is impossible to make lenses for X-rays. On the other hand it is possible to make lenses for electrons which are electrically charged and to build up an electron optics. The second consequence is that the electrons are only sensitive to strong deformations : an electron beam must pass very close to the dislocation core for the strains to be felt ; the dislocation images are therefore very narrow, but can be magnified thanks to the electron optics. The X-rays on the other hand are very sensitive to small strains and dislocation images are very wide but of the right size to be observed with the one to one magnification entailed by the absence of any lenses.

Electrons are therefore best fitted to study very thin regions containing a high density of defects while X-rays are used to study large nearly perfect crystals (up to 10^4 or 10^5 dislocations/cm^2 for instance) with no other preparation than careful polishing of the surfaces.

There are three other important differences :

a) Electrons used in microscopy are accelerated to 100 keV or more and have therefore quite short wavelengths. The corresponding Bragg angles are of the order of less than a degree and the so-called *column approximation* can be used. Bragg angles are much larger in the case of X-rays and this approximation is not valid. For the same reason, there are two reciprocal lattice points only on the Ewald sphere for X-rays, except in particular cases, while there are usually many more in the case of electrons.

b) The electrons waves used in an electron microscope are usually to a good approximation plane waves and electron micrographs are usually taken for a given departure from Bragg's law — a given value of the deviation parameter — and the observed, or simulated, contrast depends on this value. In the case of X-rays, the incident wave is a *spherical* wave. The contrast on *traverse* topographs, although it may have some similarity of appearance with that observed on an electron micrograph, is the result of an *integration*.

c) The index of refraction of matter for X-rays is slightly smaller than one. This brings about some differences with electron diffraction. One of them is that the anomalously low absorption branch of the dispersion surface is in general branch 1 for X-rays and branch 2 for electrons.

5. **Image formation of stacking faults on X-ray topographs.** — Let us consider a Borrmann triangle and a stacking fault intersecting the arms of this triangle at B_1 and C_1 (Fig. 6). When a wave-field reaches the stacking fault at a point such as q, the boundary conditions for the continuity of the tangential component of the wave-vectors must be applied along the surface of the stacking fault, just as in the case of a wave incident on a new crystal. A wave-field propagating along Aq in the first part of the crystal, and characterized by a tie-point lying on a given branch of the dispersion surface will excite in the second part of the crystal two wave-fields, one having the same tie-point, the other one with a tie-point on the other branch of the dispersion surface. We shall call the latter a *new* wave-field. The paths

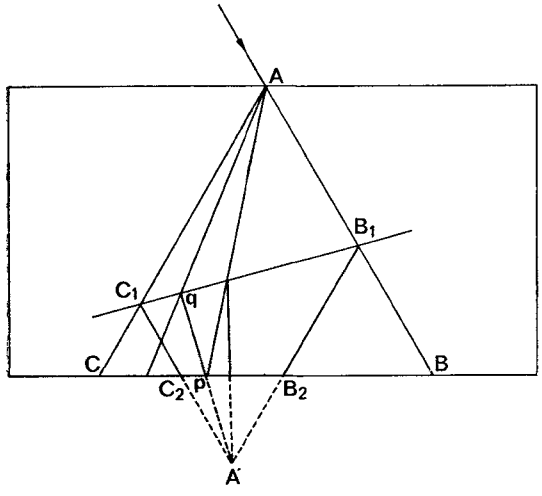

FIG. 6. — Wave-field propagation in a crystal containing a stacking fault. B_1 C_1 : stacking fault plane ; A' : focusing point of *new* wave-fields.

of the new wave-fields thus created along B_1 C_1 focalize at a point A', intersection of the parallels to the reflected and incident directions drawn from B_1 and C_1 respectively (Fig. 6). If A' lies outside the crystal it is a virtual focal point, the wave-fields breaking up into their component waves as they reach the exit surface of the crystal.

If one looks at the intensity distribution along the exit surface, there is a depletion along CC_2 and B_2 B and an enhancement along C_2 B_2. It can be shown [17] that the corresponding intensities are of the form :

along CC_2 and B_2 B : $I = I_1$
along B_2 C_2 : $I = I_1 + I_2 + I_3$

with

$$I_1 = I_{PER}(1 - |A| \sin^2 \delta/2)$$
$$I_2 = B \sin^2 \delta/2$$
$$I_3 = C \sin^2 \delta/2 + D \sin \delta$$

where I_{PER} is the intensity for the perfect crystal, δ the phase shift introduced by the stacking fault :

$$\delta = 2\pi \mathbf{h}.\mathbf{r}$$

u is the displacement vector, **h** the reciprocal lattice vector associated.

I_1 is the result of the interference between wave-fields which suffered no interbranch scattering when crossing the fault, that is wave-fields which have propagated along paths such as *Ap*. It is smaller than the corresponding intensity for the perfect crystal, I_{PER}, since part of this intensity has been used for the creation of the new wave-fields. When μt is not too large, I_1 gives rise to fringes. Equal intensity fringes are hyperbolae asymptotic to AB and AC just as in the case of the perfect crystal.

I_2 is the result of the interference between wave-fields which have all suffered interbranch scattering, that it wave-fields which have propagated along paths such as *Aqp*. It also gives rise to fringes when μt is small and equal intensity fringes are hyperbolae asymptotic to A' B_1 and A' B_2 (see Fig. 7).

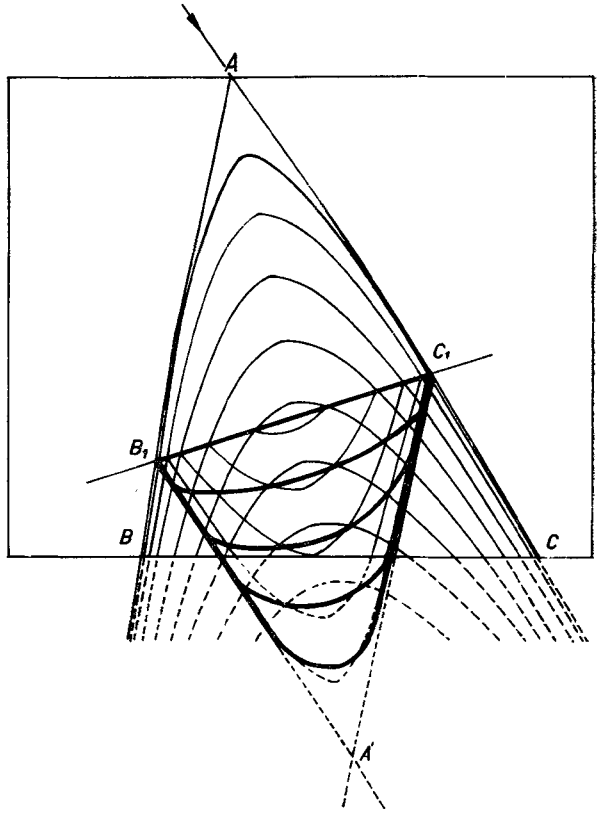

FIG. 7. — Fringes due to the interference of normal (without jumping from one branch to the other) and new (with jumping) wave-fields in the incidence plane.

I_3 is the result of the interference between wave-fields of the two latter types. That is wave-fields with paths along *Aqp* and *Ap*. It gives rise to fringes which exist even in the case of large values of μt. Figure 7 shows the shape of these interference fringes ; their period is double of the fringes due to the I_2 term.

Figure 8 shows the shape of the I_2 and I_3 interference fringes observed on the photographic plate when the stacking fault is inclined with respect to the crystal surfaces. What is observed in practice is a superposition of the two types of fringes, the I_3 fringes becoming progressively predominant when μt increases.

It will be noticed that only the second term in I_3 depends on the *sign* of the phase shift and will enable, for instance, to distinguish between intrinsic and extrinsic faults in silicon-type structures.

Figure 9 shows the result of a computer simulation for $\delta = 2\pi/3$ in the case of a stacking fault in a 400 μm thick silicon crystal, CuKα and a 111 reflection. It will be noticed that the first and last fringe have opposite contrasts and that these contrasts are exchanged, enabling the unambiguous determination of δ.

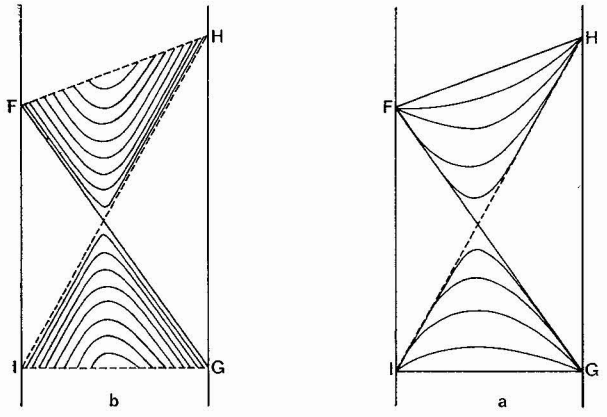

FIG. 8. — Fringes observed on a section pattern. *a*) Interferences between new fields alone (I_2 in the expression of the intensity). *b*) Interferences between normal and new fields (I_3 in the expression of the intensity).

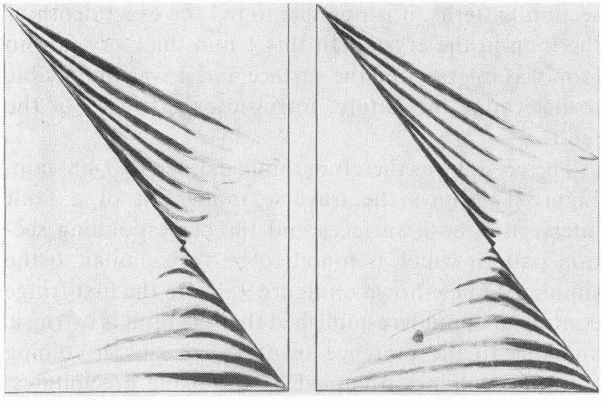

FIG. 9. — Computer simulations of the fringes observed on a section pattern in the case of 0.4 mm thick silicon crystal of (111) orientation, $\bar{1}11$ reflection ; CuKα. *a*) Fault vector 1/3 $[\bar{1}\bar{1}1]$; *b*) Fault vector 1/3 $[11\bar{1}]$.

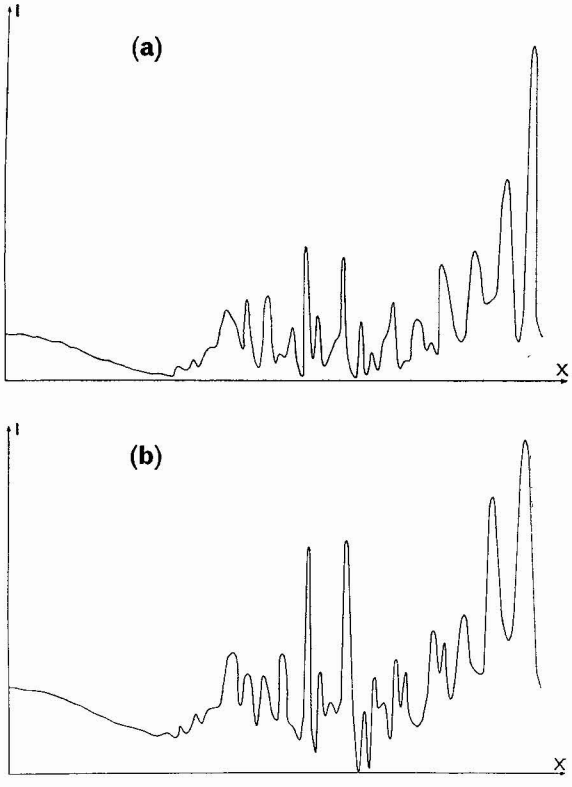

FIG. 10. — Intensity distribution across the image of a stacking fault on a *traverse* topograph. Same conditions on figure 9. *a*) Fault vector 1/3 $[\bar{1}\bar{1}1]$; *b*) Fault vector 1/3 $[11\bar{1}]$.

On a traverse pattern, however, the observed intensity is the result of an integration. The I_2 and I_3 terms give rise to equal thickness fringes. Since their periods are different, their superposition is fuzzy except for larger values of μt for which I_3 is predominant. Figure 10 shows the intensity distribution on traverse patterns corresponding to the same conditions as the section patterns of figure 9. Two things are to be noticed : the complex structure of the fringes and the fact that the first fringe has the same contrast for both $\delta = \pm 2\pi/3$. These effects are mainly due to the fact that we are dealing here with an asymmetric reflection. In the general case it is therefore not possible to determine the sign of δ from traverse patterns only and it is necessary to use section patterns.

6. **Example of a topographic study of stacking faults in silicon.** — Czochralski grown silicon always contains a certain amount of oxygen, 5×10^{17} at/cm^3 in the case of the experiments described here. This amount is usually larger than the solubility limit of oxygen at temperatures up to 1 350° (or 1 400 °C). As grown crystals therefore contain at room temperature some oxygen in supersaturation since the diffusion coefficients are too small. When these crystals are annealed at 1 000 °C precipitation of oxide occurs. Associated

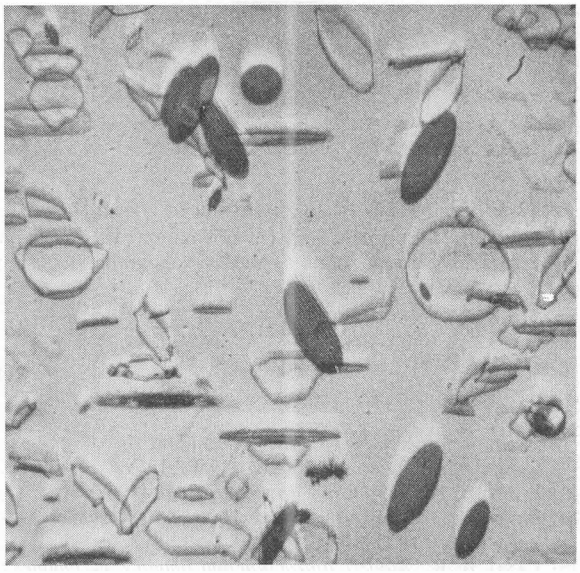

FIG. 11. — Traverse topograph of a 1 mm silicon crystal containing stacking faults and prismatic loops. (111) orientation — $\bar{1}11$ reflection, MoKα. Courtesy J. R. Patel.

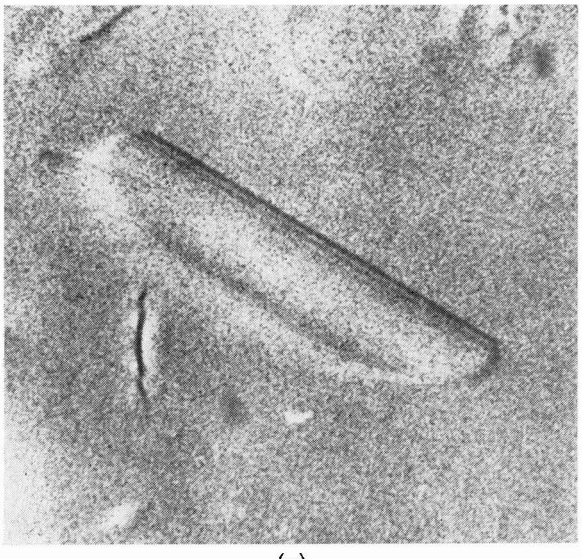

(a)

(b)

FIG. 12. — Topographs of a 0.4 mm silicon crystal showing a stacking fault. (111) orientation. $\bar{1}11$ orientation. $\bar{1}\bar{1}1$ reflection. CuKα. *a*) Traverse topograph. *b*) Section topograph. Courtesy J. R. Patel

with this precipitation is the formation of prismatic loops and stacking faults. These defects are too small to be resolved on X-ray topographs but lead to a decrease of the visibility of Pendellösung fringes and of the anomalous transmission or Borrmann effect [23-24] ; they can of course be observed and identified by electron microscopy [25]. If the crystal however is annealed at 1 200 °C, the stacking faults and prismatic loops are large enough to be observed and studied on X-ray topographs [9-10].

Figure 11 gives an example of these defects on a $\bar{1}1\bar{1}$ topograph of a 1 mm thick silicon slice of (111) orientation ; the wave-length used is MoKα. The faults are practically circular loops lying on all four (111) planes. By taking topographs with various reflections and observing the contrast at the faults and the partial dislocation surrounding them, it is easy to show that they are of Frank type with $1/3 < 111 >$ Burgers vectors. By careful study of the images observed on section patterns, it is possible to tell the exact depth of the loop in the crystal. In this 1 mm thick crystal, no loop was intersecting the surface and it was impossible to determine the nature, intrinsic or extrinsic, of the fault.

The crystal was therefore thinned down to 0.400 mm. Figure 12 shows the traverse topograph of a fault intersecting both surfaces and the corresponding section pattern which is found to be very similar to the simulated ones shown on figure 9. From the first fringe contrast it could be established that the fault is extrinsic and due to the presence of atoms of silicon coming from the volumes occupied by the oxide precipitates.

7. **Conclusion.** — X-ray topography is a powerful tool for the study of defects in crystals several square centimeters in cross section and a few tenths to a few millimeters in cross section, and containing a relatively small density of defects. It is therefore a complementary technique to electron microscopy. Although with differences mainly due to the spherical nature of X-ray waves and to the value of the wave-length, defects such as dislocations and stacking faults can be fully characterized as in the case of electron microscopy. In the case of stacking faults it is shown that the value of the phase shift can only be determined on section patterns in the general case and not on traverse patterns.

References

[1] LANG, A. R., *J. Appl. Phys.* **30** (1959) 1748.
[2] LANG, A. R., *Acta Cryst.* **12** (1959) 1959.
[3] LANG, A. R., *Advances X-ray Analysis* **10** (1967) 91.
[4] NEWKIRK, J. B., BONSE, U. and HART, M., *Advances X-ray Analysis* **10** (1967) 1.
[5] LANG, A. R., *Modern diffraction and Imaging Techniques in Materials Science*. S. Amelinckx, R. Gevers, G. Remaut and J. Van Landuyt editors (North Holland, Amsterdam) 1970, p. 407.
[6] ARMSTRONG, R. W. and WU, C. CM., in *Tools and Techniques for Microstructural Analysis*, J. L. McCall and W. M. Mueller editors (Plenum Press) 1973.
[7] KOHRA, K. and YOSHIMATSU, M., *J. Phys. Soc. Japan* **17** (1962) 1041.
[8] YOSHIMATSU, M., *Japan J. Appl. Phys.* **3** (1964) 94.
[9] AUTHIER, A. et PATEL, J. R., *Phys. Stat. Sol.* (1974).
[10] PATEL, J. R. and AUTHIER, A., *J. Appl. Phys.* (1974).
[11] YOSHIMATSU, M., *Japan J. Appl. Phys* .**4** (1965) 619.

[12] PHAKEY, P. P., *Phys. Stat. Sol.* **34** (1969) 105.
[13] LANG, A. R., *Z. Naturforsch.* **27a** (1972) 461.
[14] CHIKAWA, J. I. and AUSTERMAN, S. B., *J. Appl. Cryst.* **1** (1968) 165.
[15] AUTHIER, A. and SAUVAGE, M., *J. Physique Colloq.* **27** (1966) C3-137.
[16] KATO, N., USAMI, K. and KATAGAWA, T., *Advances X-ray Analysis* **10** (1967) 46.
[17] AUTHIER, A., *Phys. Stat. Sol.* **27** (1968) 77.
[18] VON LAUE, M., *Röntgenstrahl Interferenzen* (Akademie Verlaggesellschaft — Frankfurt am Main) 1960.
[19] AUTHIER, A., in *Advances in Structure Research by Diffraction Methods* **3** (1970) 1.
[20] KATO, N., in *X-ray Diffraction*, Edited by L. V. Azaroff (1974) p. 222.
[21] AUTHIER, A., *Advances in X-ray Analysis* **10** (1967) 9.
[22] EPELBOIN, Y., *J. Appl. Cryst.* **7** (1974) 372.
[23] PATEL, J. R. and BATTERMAN, B. W., *J. Appl. Phys.* **34** (1963) 2716.
[24] PATEL, J. R., *J. Appl. Phys.* **44** (1973) 3903.
[25] MAHER, D. M., STAUDINGER, A. and PATEL, J. R., to be published.